The Dielectrics Study of pure Graphene and Graphene/Titania/Polyvinylidene Fluoride in Giga-Hertz using Debye Relaxation Model

Abstract

A numerical approach was adopted in this study to investigate the dielectric properties, thickness and attenuation of pure graphene and Graphene/Titania/Polyvinylidene Fluoride (G4T10PVDF) in the gigahertz frequency range. The algorithms were developed and executed using the interactive environment of Maple-18 and the results were generated accordingly. The findings revealed that the dielectric constant of graphene at 15°C decreases from 20.50 to 0.22 as the frequency increases from 0.50 GHz to 99.00 GHz. Similarly, the dielectric constant of G4T10PVDF at the same temperature decreases from 40.08 to 0.48 as the frequency increases from 0.50 GHz to 99.00 GHz. This procedure was repeated at different temperatures, but the dielectric constant exhibited a similar trend across all conditions. The dielectric loss factor of pure graphene peaks at 10.24 as the frequency increases from 0.50 GHz to 10.00 GHz, while for G4T10PVDF, the loss factor reaches a maximum of 21.04 within the same frequency range. However, at higher frequencies, the dielectric losses decrease continuously. The loss tangent, thickness and attenuation values obtained were also consistent with those reported in the literature. The results indicated that pure graphene absorbs incident radiation most effectively within the frequency range of 3.0 GHz to 12.0 GHz. In contrast, the composite material of graphene/Titania/Polyvinylidene Fluoride is more effective for electromagnetic wave absorption within the frequency range of 3.0 GHz to 25.0 GHz.

Keywords: Dielectric properties; thickness; attenuation; radiation-absorbing materials; Giga-hertz

1. Introduction

Radiation-absorbing materials (RAMs) are specifically designed to reduce or eliminate the reflection of electromagnetic waves [1-2]. RAMs have the ability to absorb electromagnetic waves incident on them as effectively as possible, with minimal reflection [3]. This absorption reduces the intensity of electromagnetic waves and converts them into heat energy [4]. Radiation-absorbing materials achieve this through different mechanisms such as ohmic loss, dielectric loss, or magnetic loss, which are influenced by the material's permeability and complex permittivity [5-6].

Studies have shown that graphene possesses exceptional dielectric properties that can be used for shielding against electromagnetic wave interference and in other flexible electronics [7-8]. The dielectric behaviour of graphene is greatly influenced by factors such as doping, the presence of functional groups and layer thickness [9]. Research conducted separately by Wang et al. [10] and Dixon [11] demonstrated that materials with a higher dielectric constant, greater dielectric loss and a thicker layer are more effective at absorbing electromagnetic waves. Pure graphene and Graphene/Titania/Polyvinylidene (G4/T10/PVDF) are used as radiation-absorbing materials due to their exceptional dielectric properties, electrical conductivity and ability to absorb fast-moving particles. For instance, graphene's exceptional electrical conductivity allows it to effectively absorb and dissipate electromagnetic waves [12].

Rubrice et al. [13] studied the dielectric characteristics and microwave absorption properties of epoxy resin loaded with graphene particles in the frequency range of 2 GHz to 18 GHz. Their findings revealed that the sample loaded with the smallest graphene size of 3 μm and the highest weight ratio of 25% exhibited the highest loss tangent of 0.36 and a moderate dielectric constant (ε'=12-14) in the frequency range of 8–10 GHz. This sample also achieved the highest absorption level of 16 dB/cm at 18 GHz. Folgueras et al. [14] investigated the effect of carbon fiber fabric impregnated with polyaniline conducting polymer as radar-absorbing material within the frequency range of 8–12 GHz. Using scanning electron microscopy to analyze the results, they found that attenuation increased with frequency. The maximum attenuation value of 9 dB was obtained at 11.5 GHz, accounting for 87% absorption of the incident energy. Sallam and Mohammed [15] also examined radar-absorbing materials (RAM) within the frequency range of 0.5 GHz to 40 GHz, concluding that attenuation increased with frequency. Their study concluded that high conductivity, high permeability and increased thickness are necessary to configure an effective absorber. Huang et al. [16] explored the relative dielectric permittivity of graphene oxide (GO) under various humidity conditions at GHz frequencies. Their research observed that the relative permittivity increased with rising humidity due to water uptake.

Previous research on this subject has shown that these materials primarily attenuate electromagnetic waves through dielectric loss, while magnetic metallic components enhance impedance matching and energy loss [17]. Interestingly, most studies have focused on frequencies between 2-40 GHz and none of the available literature considers the use of Debye or Cole-Cole

relaxation methods to investigate dielectric properties. In this work, the Debye relaxation model is employed to study the dielectric properties, thickness and attenuation of graphene and G4/T10/PVDF at varying frequencies (i.e., 0.50 GHz to 99.00 GHz) and at different temperatures (15°C to 55°C). The aim is to ascertain the optimal frequency at which graphene and G4/T10/PVDF effectively attenuate electromagnetic waves. These materials are chosen due to their exceptional dielectric properties and the lack of available data on dielectric constant, loss factor, loss tangent, thickness and attenuation at higher frequencies and different temperatures for these unique radiation-absorbing materials.

2. Theoretical Framework

The four Maxwell's equations that describe the interaction between the electromagnetic fields and matter are given in their differential form as follows:

$$\nabla \times E = \frac{\partial B}{\partial t} \quad (1)$$

$$\nabla \times H = j + \frac{\partial D}{\partial t} \quad (2)$$

$$\nabla \cdot D = \rho_e \quad (3)$$

$$\nabla \cdot B = 0 \quad (4)$$

Commented [u1]: All these equations must have vector notation or vectors may be typed in BOLD

where E and H are the electric and magnetic fields respectively, D is the electric field displacement, B is the magnetic induction, j is the current density and ρ_e is the charge density [18]. The small electric field strengths D can be expressed by

Commented [u2]: Delete field, D is electric displacement

$$D = \varepsilon^* \varepsilon_o E \quad (5)$$

where ε_o is the dielectric permittivity of the vacuum and ε^* is the complex dielectric function or dielectric permittivity [19]. Research has shown that some basic atomic model used to describe the behaviour of materials in alternating field revealed that the dielectric constant under these conditions is a complex quantity [20]. The imaginary part of this complex dielectric constant determines the dielectric losses of the material.

$$\varepsilon^* = \varepsilon' - j\varepsilon'', \quad (6)$$

where ε' is the real part and ε'' is the imaginary part. ~~The ε' and ε'' parts of the dielectric~~ can be ~~derived from equation (6)~~ calculated as follows:

Commented [u3]:

whenever a dc voltage is applied to a material, polarization builds from zero to the final value. The polarization as a function of time can be written as follows:

$$P(t) = P_\infty \left(1 - e^{-t/\tau}\right), \quad (7)$$

where $P(t)$ is the polarization at any time (t), τ is the relaxation time and it is the function of temperature but independent of the time (i.e., $\omega t = 2\pi f t$). The derivative of equation (7) with time yields;

$$\frac{dP(t)}{dt} = \frac{dP_\infty}{dt}\left(1 - e^{-t/\tau}\right) = -\frac{1}{\tau}(-P_\infty)e^{-t/\tau} = \frac{P_\infty e^{-t/\tau}}{\tau} \quad (8)$$

Commented [u4]: This is not correct so can be deleted

Also from equation (7)

$$P_\infty e^{-t/\tau} = P_\infty - P(t) \quad (9)$$

Equation (9) gives

$$e^{-t/\tau} = \frac{P_\infty - P(t)}{P_\infty} \quad (10)$$

Substituting equation (10) into equation (8), we have

$$\frac{dP(t)}{dt} = \frac{P_\infty - P(t)}{\tau} \quad (11)$$

Total polarization is defined as the sum of atomic and electronic polarization i.e.

$$P_T(t) = P_a(t) + P_e(t) \quad (12)$$

The maximum value attained by the total polarization is given by:

$$P_T(t) = \varepsilon_o(\varepsilon_s - 1)E \quad (13a)$$

Commented [u5]: Not defined

$$P_e(t) = \varepsilon_o(\varepsilon_\infty - 1)E \quad (13b)$$

where ε_o and ε_∞ are the dielectric constants under direct voltage and at infinite frequency respectively. ε_∞ is defined in Maxwell's relation as $\varepsilon_\infty = n^2$. With $n^*(\omega) = n'(\omega) + in''(\omega)$. In this way the dielectric relaxation spectroscopy can be regarded as continuation of optical spectroscopy to lower frequencies [21].

The atomic polarization can be obtained from equation (13a), (13b) and (12) as follows:

$$P_a(t) = P_T(t) - P_e(t) = \varepsilon_o(\varepsilon_s - 1)E - \varepsilon_o(\varepsilon_s - 1)E$$

$$P_a(t) = \varepsilon_o\varepsilon_s E - \varepsilon_o\varepsilon_\infty E = \varepsilon_o(\varepsilon_s - \varepsilon_\infty)E \quad (14)$$

Substituting equation (14) in (11) gives

$$\frac{dP(t)}{dt} = \frac{1}{\tau}[E(\varepsilon_s - \varepsilon_\infty)\varepsilon_o - P(t)] \quad (15)$$

Expressing the problem in an alternative electric field gives

$$E = E_{max.}e^{j\omega t} \quad (16)$$

Equation (15) and (16) can be written as;

$$\frac{dP(t)}{dt} = \frac{1}{\tau}\left[E_{max}e^{j\omega t}(\varepsilon_s - \varepsilon_\infty)\varepsilon_o - P(t)\right] \quad (17)$$

Equation (17) can be solved to obtain the following expressions

$$e^{t/\tau}P(t) = \frac{e^{t/\tau}(e^{j\omega t})}{1+(j\omega\tau)} \quad (18)$$

$$P(t) = \left[\varepsilon_\infty - 1 + \frac{(\varepsilon_s - \varepsilon_\infty)}{(1+j\omega\tau)}\right]\varepsilon_o E_{max}e^{j\omega t} \quad (19)$$

Equation (19) shows that $P(t)$ is a sinusoidal function with the source frequency as the applied voltage. The instantaneous value of the flux density D is given by

$$D(t) = \varepsilon_o\varepsilon^* E_{max}e^{j\omega t} \quad (20)$$

The flux density is equal to

$$D(t) = \varepsilon_o E_{max}e^{j\omega t} + P(t) \quad (21)$$

Equating equations (20) and (21) gives

$$\varepsilon_o\varepsilon^* E_{max}e^{j\omega t} = \varepsilon_o E_{max}e^{j\omega t} + P(t) \quad (22)$$

Equation (19) and (22) gives

$$\varepsilon_o\varepsilon^* E_{max}e^{j\omega t} = \varepsilon_o E_{max}e^{j\omega t} + \left[\varepsilon_o - 1 + \frac{(\varepsilon_s - \varepsilon_\infty)}{(1+j\omega\tau)}\right]\varepsilon_o E_{max}e^{j\omega t}$$

$$\varepsilon^* = 1 + \left[\varepsilon_\infty - 1 + \frac{(\varepsilon_s - \varepsilon_\infty)}{(1+j\omega\tau)}\right] \quad (23)$$

Comparing equation (23) with equation (6) gives

Commented [u6]: n not defined

Commented [u7]:

Commented [u8]: In equation (11) P∞ not Pa(t)

Commented [u9]: alternating

Commented [u10]: Not shown how (18) & (19) derived

Commented [u11]: Electric displacement

$$\varepsilon' - j\varepsilon'' = 1 + \left[\varepsilon_\infty - 1 + \frac{(\varepsilon_s - \varepsilon_\infty)}{(1+j\omega\tau)}\right] \quad (24)$$

Solving for real and imaginary parts from equation (24) gives

$$\varepsilon' = \varepsilon_\infty + \frac{(\varepsilon_s - \varepsilon_\infty)}{(1+j\omega\tau)} + j\varepsilon'' \quad (25)$$

Setting

$$\varepsilon'' = \frac{(\varepsilon_s - \varepsilon_\infty)\omega\tau}{(1+\omega^2\tau^2)} \quad (26)$$

Substitute equation (26) in equation (25) to yield

$$\varepsilon' = \varepsilon_\infty + \frac{(\varepsilon_s - \varepsilon_\infty)}{(1+j\omega\tau)} + \frac{j(\varepsilon_s - \varepsilon_\infty)\omega\tau}{(1+\omega^2\tau^2)}$$

$$= \varepsilon_\infty + (\varepsilon_s - \varepsilon_\infty)\left[\frac{1}{(1+j\omega\tau)} + \frac{j\omega\tau}{(1+\omega^2\tau^2)}\right]$$

Electromagnetic Wave on the Surface of the RAM

The paths of an electromagnetic wave incident on the surface of the radiation-absorbing material (RAM) are shown in Figure 1. Figure 1 illustrates how the incident electromagnetic wave can be absorbed, transmitted, or reflected immediately, or internally reflected (back-reflection) when such waves strike a surface coated with RAM. However, there is some debate that the material does not absorb the incident radiation immediately, as suggested by [22], because some of the incident radiation is reflected as soon as it collides with the RAM. The schematic diagram below clearly illustrates the paths of the electromagnetic wave incident on the RAM surface.

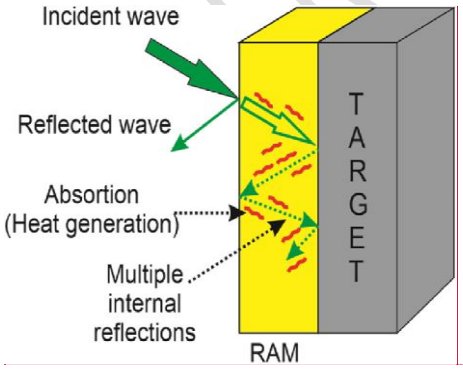

Figure 1: Schematic diagram of absorption and multiple reflections of RAMs as attenuation mechanisms [23-24].

Commented [u12]: Comparing real & imaginary parts on both sides

Commented [u13]: This expression should have real part only

Commented [u14]:

Commented [u15]: Wrong, should have real part only

Commented [u16]: No emphasis was given to the angle of incidence of wave and multiple internal reflections in the theory

3. Method

In this work, the algorithms were developed in the interactive environment of Maple-18 and the dielectric constant, loss factor, dielectric loss angle and attenuation of graphene and G4/T10/PVDF were simulated at different temperatures. The simulation was performed at various temperatures because the amount of electromagnetic radiation an object emits depends primarily on its temperature. The experimental data for the electrical conductivity, relaxation time and static permittivity of the materials (graphene and G4/T10/PVDF) were adopted from [13; 25-26] and substituted into the written algorithms. The dielectric properties, thickness and attenuation of graphene and G4/T10/PVDF were obtained based on the assumption that the transient polarization can be represented by a simple exponential with a single relaxation time.

The electrical conductivity, relaxation time at different temperatures and static permittivity were substituted into the written algorithms using derived equations (26) and (27). Lanagan [27] relates the dielectric and loss factor using the following equation.

$$\tan\delta = \frac{\varepsilon''}{\varepsilon'} \tag{28}$$

Meanwhile according to Yakut et al., [28] the dielectric constant, ε' and thickness, μ of the material is related as thus:

$$\mu = \frac{\varepsilon' \varepsilon_o A}{C}, \tag{29}$$

ECE 3300 LAB 1b [29] establishes the relationship between attenuation coefficient α, the dielectric constant, loss factor, the electrical conductivity and frequency as thus:

$$\alpha = \omega\left\{\frac{\sigma\varepsilon'}{2}\left[\sqrt{1+\left(\frac{\varepsilon''}{\varepsilon'}\right)^2}-1\right]\right\}^{1/2} \tag{30}$$

The simulation using equations (26) to (30) was performed at different temperatures and frequencies in order to investigate the impact of dielectric constant, loss factor, loss tangent, thickness and attenuation on the RAM.

4. Results and Discussion

4.1 Dielectric Constant of Graphene and Graphene/Titania/Polyvinylidene

The dielectric constant of both graphene and graphene/titania/polyvinylidene, as presented in Figure 2 (a) and (b), was obtained from equation (27). The relaxation frequencies were calculated

Commented [u17]: Give values adopted

Commented [u18]: For which condition?

Commented [u19]: A and C not defined

Commented [u20]: ?

Commented [u21]: Not a single expression shows temperature variation. If any write expression involving temperature

using the relation τ = (2πf_r)^(-1). The results of the dielectric constant versus frequency revealed an increase in the dielectric constant for both graphene and G4/T10/PVDF as the temperature increased from 15°C to 55°C. However, the behaviour of the dielectric constant was not the same with increasing frequency. The dielectric constant was higher at lower frequencies but decreased as the frequency increased. This is because the real part of the permittivity (the dielectric constant) is frequency-dependent [30] and the overall conductivity, which consists of different conduction mechanisms such as orientational, interfacial, electronic and ionic polarization that contribute to the dielectric constant, is also frequency-dependent. The most prevalent mechanism is ionic conductivity, which varies inversely with frequency.

Commented [u22]: Write properly

The decrease in the dielectric constant with increasing frequency at all temperatures may be due to the fact that the dipoles cannot keep up with the rapid changes in the applied field. This decrease in the dielectric constant as frequency increases suggests that not all four types of polarization contribute to the dielectric constant at higher frequencies [27-28].

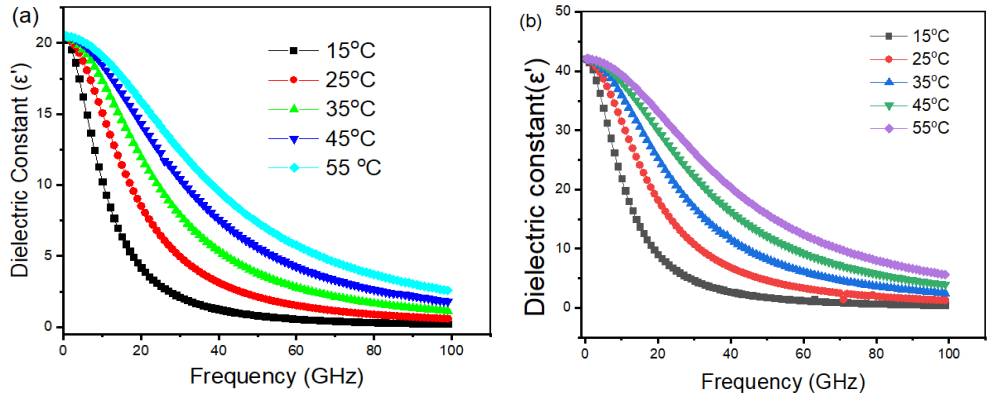

Figure 2: Frequency dependence of dielectric constant (ε') of (a) Graphene and (b) G4/T10/PVDF at indicated temperatures

4.2 Dielectric Loss Factor

The results obtained from equations (26) and (27) were used to generate the Cole-Cole plots. Each dielectric loss factor and its corresponding dielectric constant at a specific temperature were copied from an Excel sheet and pasted into the Minitab worksheet. The columns for both dielectric

constant and loss factor for each temperature were highlighted in the Minitab worksheet and the scatter plot option from the Minitab software was used to create the Cole-Cole plots. The Cole-Cole plot for dielectrics with a simple relaxation time is a semi-circle (Figure 4a and Figure 4b) and our results agree with previous studies [36-38]. This plot is a standard method for determining whether a system has a single relaxation time and thus, the data can be fitted using the Debye relaxation method.

Commented [u23]: Show their results on your plot or give in table

The Cole-Cole plots in this work show that the data for graphene and G4/T10/PVDF can indeed be fitted to Debye equations. The Cole-Cole plot is also useful for characterizing different types of distribution functions.

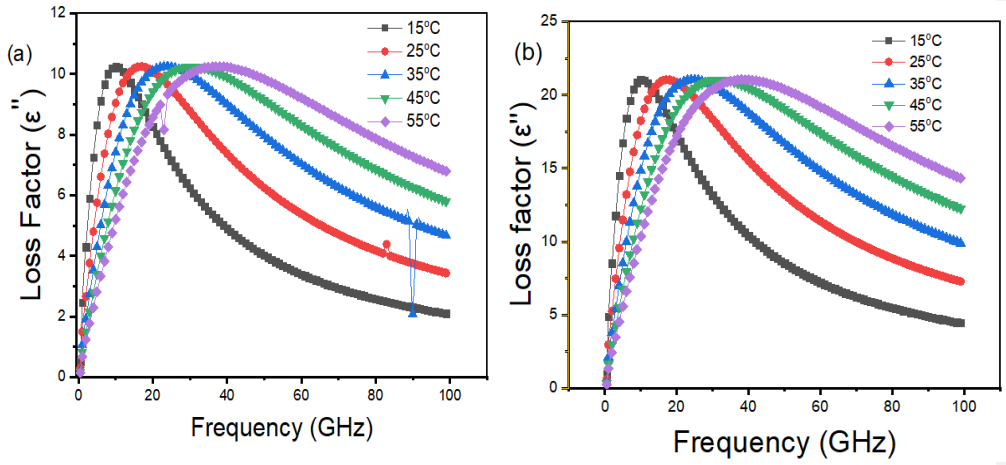

Figure 3: Frequency dependence of loss factor (ε'') of (a) Graphene and (b) G4/T10/PVDF at indicated temperatures

4.3 Cole-Cole Plot

The results obtained from equations (26) and (27) were used for the Cole-Cole plots. Each dielectric loss factor and the corresponding dielectric constant at a particular temperature were copied from excel sheet and pasted in Minitab worksheet. The columns for both dielectric constant and loss factor for each temperature were highlighted in the Minitab worksheet and the scatter plot option from the Minitab software graph were used to the Cole-Cole plots. The Cole-Cole plot for

dielectric with a simple relaxation time is a semi-circle (Figure 4a and Figure 4b) and our results of the Cole-Cole diagrams have agreed with previous works [36-38]. This plot is a standard method of finding out whether a system has a single relaxation time and hence, the data can be fitted using Debye relaxation method. The Cole-Cole plots in this work, show that data for graphene and G4/T10/PVDF can indeed be fitted in Debye equations. The Cole-Cole plot is also useful for the characterization of different types of distribution functions.

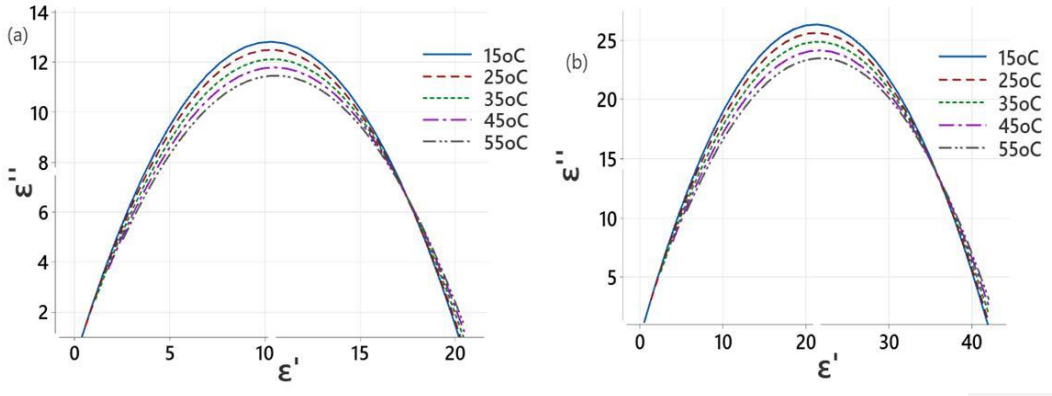

Figure 4: The plots of $\varepsilon''(\omega)$ against $\varepsilon'(\omega)$ in Cartesian coordinates for (a) Graphene (b) G4/T10/PVDF

Commented [u24]: What it means. In fig degree should be super script
Specify the value of ω

4.4 The Loss Tangent

The ratio of the dielectric loss factor, ε" to the dielectric constant, ε', was plotted using equation (28), as shown in Figure 5 (a) and (b). The loss tangent provides information about the energy expended in a given sample to store electric charges [39]. Figure 5 (a) and (b) show the energy dissipation or frequency-dependent loss tangent of graphene and G4/T10/PVDF. At a low frequency (i.e., 0.5 GHz) and a temperature of 15°C, the loss tangent of graphene was 0.0234, steadily increasing to 9.679 at the highest frequency (i.e., 99.0 GHz). The loss tangent decreases as the temperature increases. G4/T10/PVDF exhibits a similar behaviour for the same frequency and temperature. For instance, at 0.5 GHz and 15°C, the loss tangent of G4/T10/PVDF increases from 0.0235 to 9.3418. This small value of the loss tangent at low frequency may be due to the high value of the dielectric constant, ε'. This behaviour of the loss tangent is consistent with

literature [40-41]. The lower tan δ at lower frequencies and the larger tan δ observed at higher frequencies indicate that more of the original signals are transmitted, while more dielectric absorption occurs at higher frequencies [42].

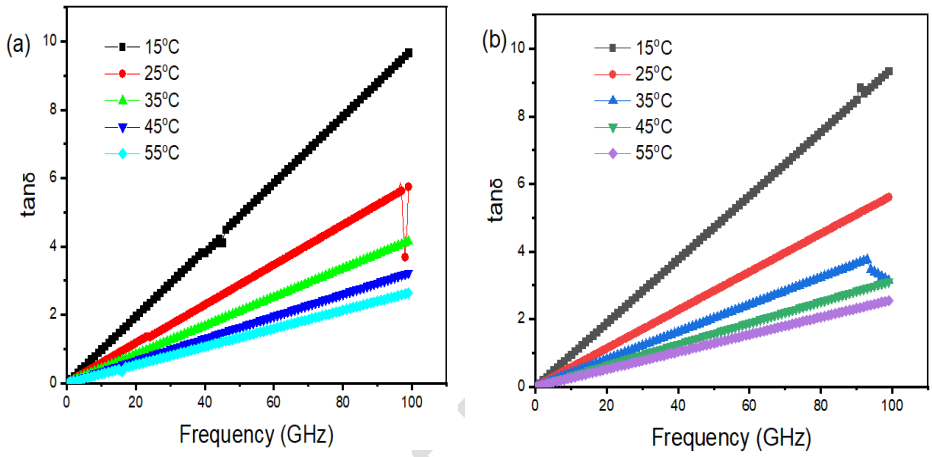

Figure 5: The loss tangent against the frequency (a) Graphene and (b) G4/T10/PVDF at different temperatures

4.5 Frequency- dependent of the Attenuation

Equation (30) clearly shows that the attenuation coefficient, α, is proportional to the square root of the frequency, meaning that as the frequency increases, the attenuation coefficient also increases. The results presented in Figures 6 (a) and (b) reveal that the attenuation coefficient of graphene at 15°C increases from 0.18 dB to 7.20 dB as the frequency rises from 0.5 GHz to 99 GHz, while that of graphite increases from 0.28 dB to 10.69 dB at the same temperature. The attenuation coefficients for the other temperatures studied in this work (i.e., from 25°C to 55°C) exhibit similar behaviour as the frequency varies for each temperature. This increase in the attenuation coefficient with frequency is consistent with other works reviewed [43-44]. The increase in the attenuation coefficient as temperature rises may be due to the decrease in the relaxation time of the materials, as temperature is inversely proportional to relaxation time.

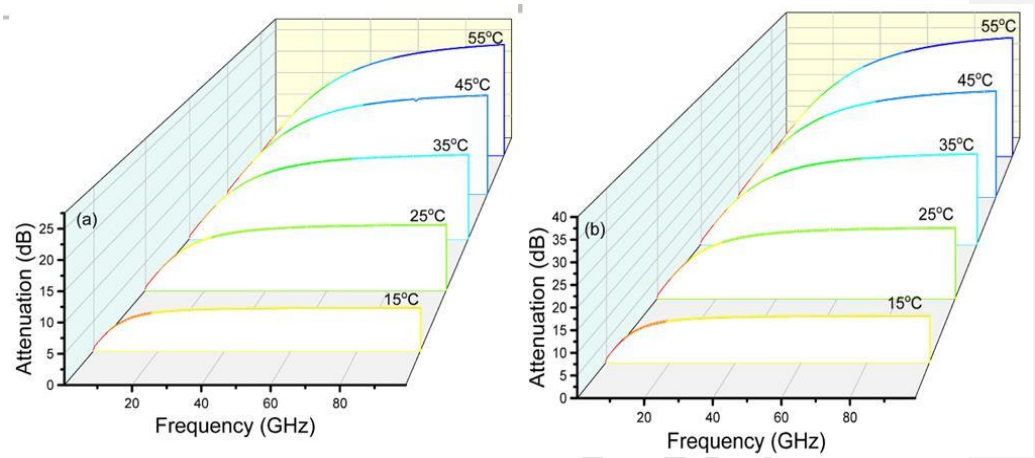

Figure 6: Frequency dependency of the attenuation of (a) Graphene and (b) G4/T10/PVDF at the indicated temperatures

4.6 The Relaxation Spectrum of the Materials

The relaxation spectrum of graphene is shown in Figure 7a and that of G4/T10/PVDF is depicted in Figure 7b, both as functions of frequency at different temperatures. The dispersion curves reveal a decrease in the real permittivity, ε', as the frequency increases, while the absorption curves show peaks in the imaginary permittivity, ε". The dispersion and absorption curves for the materials studied in this work are consistent with the findings of the reviewed literature [45-49].

Commented [u25]: Show others results on your plot or give in table

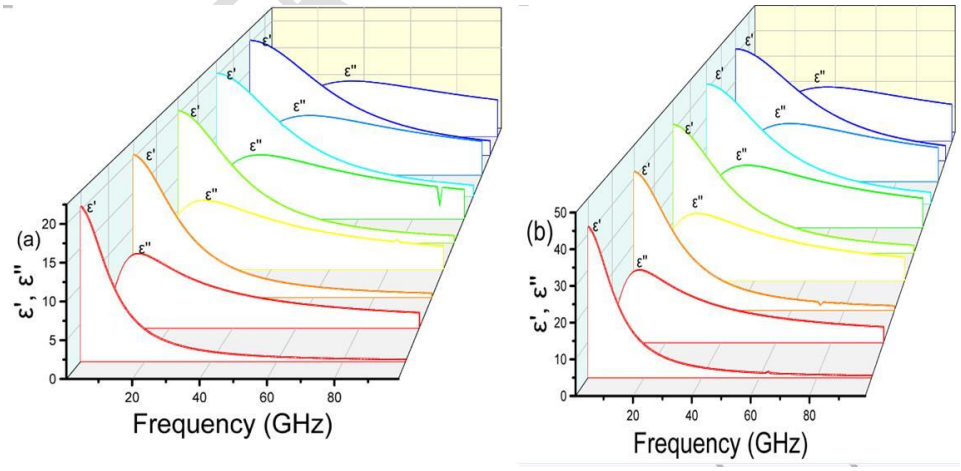

Figure 7: Frequency dependency of the dielectric constant (ε') and loss factor (ε'') of (a) Graphene and (b) G4/T10/PVDF

4.7 Thickness of the Materials

The relaxation spectrum of graphene is shown in Figure 7a and that of G4/T10/PVDF is depicted in Figure 7b, both as functions of frequency at different temperatures. The dispersion curves reveal a decrease in the real permittivity, ε', as the frequency increases, while the absorption curves show peaks in the imaginary permittivity, ε''. The dispersion and absorption curves for the materials studied in this work are consistent with the findings of the reviewed literature [45-49].

Commented [u26]: Text repeated instead of description of figure 8

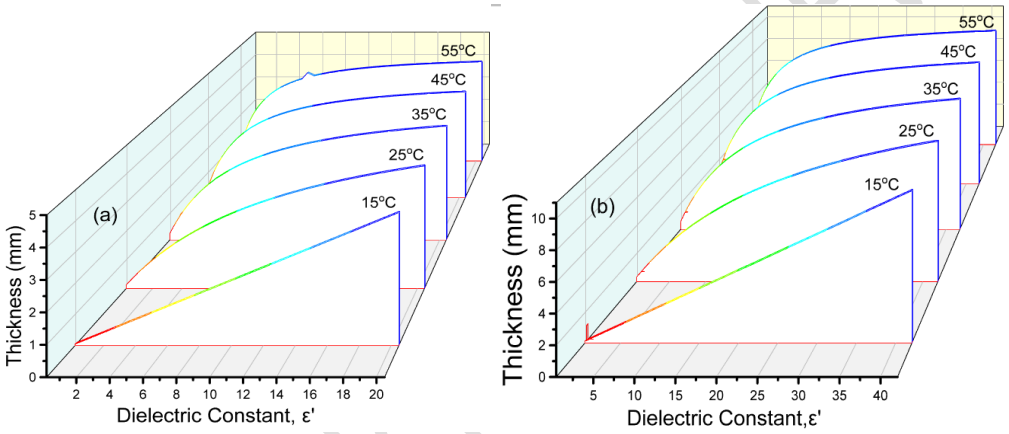

Figure 8: The behaviour of Thickness against the dielectric constant at different temperatures (a) Graphene (b) G4/T10/PVDF

5. Conclusion

In this work, the algorithms were developed using Debye relaxation equations and their relationship with material thickness and attenuation in the interactive environment of Maple-18. The results obtained from the algorithms revealed that the dielectric constants of the materials studied were higher at low frequencies (i.e., 0.5 GHz to 4.5 GHz) and the dielectric constant decreased as the frequency increased. Since a higher dielectric constant indicates greater storage of electrical energy, this implies that more electromagnetic waves are absorbed at lower frequencies. The effect of temperature on the dielectric constant was also examined, revealing that

the dielectric constant increased with rising temperature. This suggests that the materials studied absorb more electromagnetic waves at higher temperatures.

The influence of frequency and temperature on the dielectric loss factor of the materials was also analyzed. The results showed an increase in the loss factor up to its maximum value as both frequency and temperature increased. However, the loss factor decreased with further increases in frequency. The maximum or peak value of the loss factor indicates that graphene is most effective as an absorber at 8-12 GHz, while G4/T10/PVDF is most effective at 3-14 GHz. Temperatures of 25°C and above for the RAMs studied here are optimal for electromagnetic wave absorption.

The data generated in this study were plotted using Cole-Cole plots to determine whether graphene and G4/T10/PVDF exhibit a single relaxation time. The semi-circular plots shown in Figure 3 indicate that the data can be modeled using Debye relaxation equations. The thickness of graphene and G4/T10/PVDF was also studied, as microwave absorbers change their dielectric properties with thickness. The results show that lower frequencies and higher temperatures correspond to greater thicknesses. Additionally, the attenuation of graphene and G4/T10/PVDF increased with both frequency and temperature.

The findings of this work are consistent with experimental data as well as with the reviewed literature. This study also explored higher frequencies and temperatures beyond those previously examined. The significance of this work is to confirm whether the data for graphene and G4/T10/PVDF can be fitted using Debye relaxation equations, to verify the accuracy of the numerical approach in replicating experimental data and to extend the analysis to higher frequencies and temperatures beyond those reviewed in the literature.

Commented [u27]: Not given

6. REFERENCES

[1]. Kim, S., Lee, S., Zhang, Y., Park, S., & Gu, J. Carbon-Based Radar Absorbing Materials toward Stealth Technologies, *Adv. Sci.***10**(32), https://doi.org/10.1002/ advs.202303104

[2]. Yuzcelik, C.K. Radar absorbing material design, Calhoun: The NPS Institutional Archive, (2003), http://www.nps.edu/library

[3]. Wang G. Absorbing Materials and Their Applications in Electromagnetic Compatibility Design of Mobile Phones, **18 (34)** (2010)**,** 62-66.

[4]. Gu, J., Lv, Z.,Wu, Y., Guo,Y., Tian, L., Qiu, H., Li, W., Zhang, Q. Dielectric thermally conductive boron nitride/polyimide composites with outstanding thermal stabilities via in-situ polymerizationelectrospinning-hot press method, *Composites: Part*, **94**(2017) 209-216; http://dx.doi.org/10.1016/j.compositesa.2016.12014.

[5]. Huang, L., Liu, X., Yu, R. Enhance Microwave Absorption Properties of Rod- Shaped Fe_2O_3/Fe_3O_4/ MWCNTs composites, *Prog. Nat. Sci.: Mater.Int'l,***28**(2018), 288- 295,

[6]. Zhao, L., & Zhao, T. Research on Design and Application of Absorbing Material Based On Electromagnetic Compatibility of Handheld Device, *IOP Conf. Ser.: Mater. Sci. Eng*. **677** (2019) 022016

[7]. Arya, A. Dielectric Properties of Graphene: An Overview Chapter, (2024). https://www.researchgate.net/publication/378941165

[8]. Li, J., Li, J. Li, T., Xu, Z., Chen, Y., Zhang, L., Qi, Q., Liang, B. and Meng, F. Flexible and excellent electromagnetic interference shielding film with porous alternating PVA-derived carbon and graphene layers, *iScience*, **26**, 107975, (2023). http://creativecommons.org/licenses/by-nc-nd/4.0/

[9]. Prokhorov, E., Barquera-Bibiano, Z., Manzano-Ramírez, A., Luna-Barcenas, G., Kovalenko,Y., Hernández-Landaverde, M. A., ... & Vargas, J. H. New insights in graphene oxide dielectric constant. *Materials Research Express*, *6*(8), (2019), 085622.

[10]. Wang, C., Li, J., & Guo, S. High-performance electromagnetic wave absorption by designing the multilayer graphene/thermoplastic polyurethane porous composites with gradient foam ratio structure, *Composites Part A*, **125**. (2019). www.elsevier.com/locate/compositea.

[11]. Dixon, P. Impact of TIM Dielectric Constant on EMI Radiation, Laird Thermal Materials, (2020).

[12]. Radiation Physics. https://courses.lumenlearning.com>14-7radiation . Assessed on 15/02/2024

[13]. Rubrice, K., Castel, X., Himdi, M., Parneix, P. Dielectric Characteristics and Microwave Absorption of Graphene Composite Materials, *Mater*., **9** (2016) 825; doi: 10.3390/ma9100825

[14]. Folgueras, L.C., Nohora, E.L., Farez, R., & Rezende, M.C. Dielectric Microwave Absorbing Material Processed by Impregnation of Carbon Fiber Fabric with Polyaniline, *Mater.Research*, **10(1)**, (2007) 95-99.

[15]. Sallam, T.M., Mohammad, A.R.M. On the Radar Absorbing Material Reflectivity and Electromagnetic Interference Shielding Effectiveness, (2022), TechRxiv. Preprint. https://doi.org/10.36227/techrxiv.21086998.v1

[16]. Huang, X., Leng, T., Georgiou,T., Abraham, J., Nair,R. R., Novoselov, K. S., & Hu, R. Graphene Oxide Dielectric Permittivity at GHz and Its Applications for Wireless Humidity Sensing, *Sci. Reports*, **8**,(2018), 43, www.nature.com/scientificrepoets/

[17]. Qin, M., Zhang, L., & Wu, H. Dielectric Loss Mechanisms in Electromagnetic Waves Absorbing Materials, *Adv. Sci.*, **9**, (2022)-VCH GmbH

[19]. Pramanik, A. Electromagnetism; Theory and Applications, Prentice-Hall of India Private Limited, (2006) New Delhi-11000

[20]. Onimisi, M.Y. & Ikyumbur, J.T. Comparative Analysis of Dielectric Constant and Loss Factor of Pure Butan-1-ol and Ethanol, *ajcmp*,**5(3)**,(2015) 69-75; http://journal.sapub.org/ajcmp

[21]. Kremer, F. and Schonhas, A. Broadband Dielectric Spectroscopy, Library of Congress Cata loging-in-publication data, Springer-Verlag Berlin Heidelberg, (2003).

[22]. Dhawan, S.K., Singh, N., Venkatachalam, SShielding effectiveness of conducting polyaniline coated fabric at 101GHz, *Synthetic Metals*, **12(2)**, (2002), 389- 393.

[23]. Ruiz-Perez, F., Lopez-Estrada, S.N., Tolentino-Hernandez, R.V., & Caballero-Briones, F. Carbon-based radar absorbing materials: A critical review, *J. Sci.: Adv. Mater. Dev.*, **7**, (2022), 100454

[24]. Elmahaishi,M.F., Azis, R.S.,Ismail, I., Muhammad, F.D. A review on electromagnetic microwave absorption properties: their materials and performance, *jmr & t*, **20**, (2022), 2188-2220; https://doi.org/10.1016/j.jmrt.2022.07.140

[25]. Rani, P., Dubey, G.S. and Jindal, V.K. (2014). DFT study of optical properties of pure and doped Graphene, *Physical E Low-dimensional Systems and Nanostructures*, **62**, 28-32,

[26]. Ishaq, S., Kanwal, F., Atip, S., Moussa, M., Azhar, U., & Losic, D. Dielectric Properties of Graphene/Titania/Polyvinylidene Fluoride (G/TiO_2/PVDF) nanocomposites, *Mater.*, **13(205),** (2020), 1-11. www.mdpi.com/journal/materials

[27]. Lanaga. M. Dielectric Properties and Metamaterials, Materials Research Instititude Penn State University, Kyoto Japan, (2008)

[28]. Yakut, S., Ulutas, K. and Deger, D. (2019). Effect of thickness on the dielectric properties and glass transition of plasma poly (ethylene oxide) thin films, *Materials Science & Engineering C*, 104, 109962.

[29]. ECE3300 LAB 1b, Dielectric Materials and Attenuation **2,** https://utah.instructure.com>files>download . Assessed on 11/01/2024.

[30]. Arshad, M. Khan, M.A., Rasool, R.T., Arshad, M.I., Javed, Z. Hayat, S., Ilyas, S.Z. (2024). Structural, Physiochemical and Electrical Properties of Co2Y-type barrium hexaferrites, *Ceramics International*, **50**, 23047-23057

[31]. Zhai, D. Zhang, F.,Wei, C., Bai, Y., Zhu, L., Li, G., Shanga,X., Suna,J., Chend, J., Liu, M., Peng, J.,Gu,H. Dielectric properties and electromagnetic wave transmission performance of polycrystalline mullite fiberboard at 2.45 GHz, *Cer. Int'l*, **46** (2020), 7362-7373

[32]. Sani, Y., Azis, R.S., Ismail, I., Yaakob, Y., Mohammed, J. Enhanced electromagnetic microwave absorbing performance of carbon nanostructures for RAMs: A review, *Appl. Surf. Sci. Advs.*, **18**, (2023), 100455

[33] Parkman, T. Measuring Damping Performance using a High-Frequency Dynamic Mechanical Analyzer, (2022), https://ctherm.com>resources>newsroom>dma>dam . Assessed on 19/02/2024

[34]. Gayer, R.G. Dielectric characterization and reference material, NIST Technical Note 1338

[35]. Ahmad, M.M., Kot, H.M., Joseph, C., Kumar, S. and Alshoaibi, A. Transport and Dielectric Properties of Mechanosynthesized $La_{2/3}Cu_3Ti_4O_{12}$ *Cer., Cryst.*, ***11*(3)**, (2021), 313, https://doi.org/10.3390/cryst11030313

[36]. Piyasena, P., Dussault, C., Koutchma, T., Ramaswamy, H.S. & Awuah, G.B. Radio Frequency Heating of Foods: Principles, Applications and Related Properties—A Review, *Crit. Rev. F. Sci. Nutr.*, **43(6)** (2003):587– 606

[37]. Wei, Y. and Sridhar, S. A new graphical representation for dielectric data, *J. Chem. Phys*. **99 (4),** 15, http://ojps.aip.org/jcpo/jcpcr.jsp

[38]. Musa N. Onimisi M. Y., Ikyumbur J. T. Frequency and Temperature Dependence of Ethanol Using the Cole-Cole Relaxation Model, *American J. Cond. Matter Phy.*, 10(2) (2020): 44-49, http://journal.sapub.org/ajcmp

[39]. Javed, Z., Rasool, R.T. Alhummiany, H. Majeed, A. Gulbadan, S. Ashraf, G.A., Al-Anazy, M. Irfan, M. Yousuf, E., Akhtar, M. N., Arshad, M., Khan, M.A. (2024) Structural Morphological, dielectric and Spectral Properties of SrMg-Ho X-type Magnetic nanomaterials suitable for microwave absorption application. *Vacuum, 222*, 112965

[40]. Kasap, S.O. Principles of Electronic Materials and Devices, 3rd Edition, McGraw-Hill, (2005).

[41]. Baker-Jarvis, J., Janezic, M.D., Riddle, B. & Holloway, C.L. Dielectric and Conductor-Loss Characterization and Measurements on Electronic Packaging Materials, National Institute of Standards and Technology Technical Note 1520, (2001).

[42]. PCB Stack up Design Considerations for Intel® FPGAs, https://www.intel.com>docs>programmable>contents . Assessed on 13/01/2024

[43]. Ni, C., Wu, D., Xie, X., Wang, B., Wei, H., Zhang, Y., Zhao, X., Liu, L.,Wang, B., & Du, W. Microwave absorption properties of microporous CoNi@(NiO-CoO) nanoparticles through dealloying. *J. Mag. & Mag. Mater*., **503** (2020)

[44] Liu, X., Xiong, F., Xie, Q., Yang,X., Chen, D. and Wang, S. Research on the Attenuation Characteristics of High-Frequency Elastic Waves in Rock-Like Material, *Mater*.,15(19), (2022) , 6604

[45]. Shah, D.D., Mehta, P.K., & Panchal, C.J. Structural Microstructural and Electrical Transport Studies of Ba ($Fe_{0.25}$ $Eu_{0.25}Nb_{0.5}$) O_3, *J.Nano.& Elect. Phy.*, **5(2)**, (2013), 02022 (4pp)

[46]. Rayssi, Ch. El.Kossi, S., Dhahri J. & Khirouni, K. Frequency and temperature-dependence of dielectric permittivity and electric modulus studies of the solid solution $Ca_{0.85}Er_{0.1}Ti_{1-x}Co_{4x/3}O_3(0 \leq x \leq 0.1)$, *RCS. Adv.* **8**, (2018) 17139

[47]. Liu, H., Jie, T., Li, B., Youming, D., & Chunning, Q. Study of the low-frequency dispersion of permittivity and resistivity in tight rocks, *J. Appl.Geophy.*, **143** (2017), 141-148

[48]. Abbas, S.M., Chandra, M., Verma, A., Chatterjee, R., Goel, T.C. Complex permittivity and microwave absorption properties of a composite dielectric absorber, *Composites: Part A* **37** (2006) 2148–2154

[49]. Bijwe, D.R., S.S. Yawale, S.S., Kumbharkhane, A.C., Pengd, H., Yawaleean, D.S., Yawale, S.P. Complex dielectric behaviour of doped polyaniline conducting polymer at microwave frequencies using time domain reflectometry, *Rev. Mexi. de Fis.* **65(6)** (2019) 590–600, https://doi.org/10.31349/RevMexFis.65.590

[50]. Shorstkii, I. & Sosnin, M. Microwave absorption and reflection properties of a composite dielectric absorber, *IOP Conf. Ser.: Mater. Sci. Eng.* **564** (2019) 012041